IOPscience iopscience.iop.org

Home Search Collections Journals About Contact us My IOPscience

An exact transmission coefficient with one and two barriers in graphene

This article has been downloaded from IOPscience. Please scroll down to see the full text article.

2013 J. Phys. A: Math. Theor. 46 155304

(http://iopscience.iop.org/1751-8121/46/15/155304)

View the table of contents for this issue, or go to the journal homepage for more

Download details:
IP Address: 79.109.63.188
The article was downloaded on 03/04/2013 at 20:56

Please note that terms and conditions apply.

IOP PUBLISHING JOURNAL OF PHYSICS A: MATHEMATICAL AND THEORETICAL

J. Phys. A: Math. Theor. **46** (2013) 155304 (20pp) doi:10.1088/1751-8113/46/15/155304

An exact transmission coefficient with one and two barriers in graphene

J D Lejarreta[1], C H Fuentevilla[1], E Diez[2] and José M Cerveró[2]

[1] Departamento de Física Aplicada, Universidad de Salamanca, E-37008 Salamanca, Spain
[2] Departamento de Física Fundamental, Universidad de Salamanca, E-37008 Salamanca, Spain

E-mail: cervero@usal.es

Received 10 December 2012, in final form 5 March 2013
Published 3 April 2013
Online at stacks.iop.org/JPhysA/46/155304

Abstract
In this work, we find the exact transmission coefficient across one and two potential barriers in graphene. We obtain theoretical expressions for this coefficient in terms of the characteristics of the potential barriers, height, width and separation and the characteristics of the carriers, Fermi energy and incidence angle. This coefficient is essential in order to characterize the conductance in several electronic devices based on graphene. Since the calculated transmission coefficient is highly non-isotropic, we extend the Landauer formalism and obtain a closed expression for transistor conductance.

PACS numbers: 03.65.Xp, 03.675.Ss, 72.20.i, 72.20.Fr

(Some figures may appear in colour only in the online journal)

1. Introduction

Graphene is a new material isolated a few years ago by Andre Geim and his group at the University of Manchester [1]. The graphene band structure presents no gap energy [2, 3] (we simply consider ideal graphene without impurities) between the valence and conduction bands, and the special relationship of linear scattering [4], the energy–momentum in the bands, converts the graphene into a material very different from conventional semiconductors. Electrons in graphene appear to behave like massless relativistic particles, giving graphene *high electronic mobility* at room temperature. These very unusual properties lead us to expect that the transport characteristics of graphene, and, in particular, the *transmission coefficient* will be very different from traditional semiconductors, and it seems natural that traditional quantum mechanics, based on the Schrödinger equation, is unable to explain such unusual properties [5]. Electrons in graphene without impurities are present as ultrarelativistic particles and must be described by means of the Dirac ultrarelativistic equation [1, 6].

The transmission coefficient of an ultrarelativistic particle through a potential barrier in a graphene monolayer was addressed in [7] by means of a simplified formula, and in [8] by

 © 2013 IOP Publishing Ltd Printed in the UK & the USA

the matrix-T standard method. By means of computational calculations, this work estimates numerically its transmission probability in a one-dimensional barrier of various shapes.

Transport phenomena in graphene have also been studied in [9–15], where the Klein tunnel effect is justified and the role of charged impurities and their concentrations, which cause scattering of the carriers and largely affect transport, has been considered in [16], and the electronic transmission through a resonant double barrier has been considered in [17, 18]. In [19], this problem is treated by means of the associated Green functions.

The *transmission coefficient* is a necessary step in order to calculate the intensity of the electric current or conductance in various electronic devices of interest [20], such as filters or graphene superlattices [21], with or without disorder [22]. It seems that carrier transport through these devices is highly anisotropic, suggesting the possibility of building electronic circuits without cutting or etching. Our interest is focused on obtaining an analytical expression of this *transmission coefficient* for different types of potential barriers. Although we have used a direct method of calculation to obtain exact analytical expressions, other approaches can indeed be used, such as the well-known S-matrix method, also known as the transfer matrix formalism that can be even more appropriate in the case of multiple barriers.

2. The band structure and the features of graphene

Graphene is a material that seems to consist of a sheet of carbon atoms only one atom thick, arranged in the vertices of regular hexagons forming a honeycomb structure [2]. This two-dimensional structure is the cause of the remarkable structural flexibility of graphene, which is reflected in its electronic properties.

The carbon atom in sp^2 hybridization gives a flat trigonal structure supported by type σ C–C links that each atom sets with three neighboring atoms [9]. Thus, a hexagonal structure with localized bonds is generated, providing a very robust material. The unhybridized p_z atomic orbitals are arranged perpendicular to this structure, one per carbon atom. The overlapping of these orbitals between neighboring atoms leads to the formation of π-type bonds, whose electrons become delocalized through the graphene sheet.

The study of the band structure in graphene has been known since the work of Wallace [3] in 1947, who, using the approximation of tightly bound electrons that can jump only between neighboring atoms located no more than two atoms away, managed to establish for the first time the band structure of graphene. This structure is described in its current form in [4]. N p_z electrons from the carbon, one per atom in the crystal, spread over the network with pseudomomentum or wave vector $\mathbf{k}$ remaining in two energy bands given by

$$E_{\pm}(\mathbf{k}) = \pm t\sqrt{3 + f(\mathbf{k})} \tag{1}$$

$$f(\mathbf{k}) = 2\cos(\sqrt{3}k_y a) + 4\cos\left(\frac{\sqrt{3}}{2}k_y a\right)\cos\left(\frac{3}{2}k_x a\right). \tag{2}$$

Formula (1) describes the energy of the electrons in both the conduction band, sign $+$, and the valence band, sign $-$, for graphene. In (1), $t \approx 2.8$ eV is the interaction energy between the electron of a carbon atom and the neighboring one and $a \approx 1.42$ Å is the C–C distance.

There are two points in the graphene reciprocal network, with wave vectors $\mathbf{K}$ and $\mathbf{K}'$,

$$\mathbf{K} = \left(\frac{2\pi}{3a}, \frac{2\pi}{3\sqrt{3}a}\right) \qquad \mathbf{K}' = \left(\frac{2\pi}{3a}, -\frac{2\pi}{3\sqrt{3}a}\right), \tag{3}$$

in which $f(\mathbf{K}) = f(\mathbf{K}') = -3$ and the energy of both is identically zero. These points are called *Dirac points* and, if we consider only a region in the momentum space close to any

of these Dirac points, $\mathbf{k} = \mathbf{K} + \mathbf{q}$ or $\mathbf{k} = \mathbf{K}' + \mathbf{q}$, then the energy in each band may be approximated by

$$E_{\pm}(|\mathbf{q}|) = \pm\frac{3}{2}at\sqrt{q_x^2 + q_y^2} + O\left[\frac{|\mathbf{q}|^2}{|\mathbf{K}|^2}\right] = \pm\hbar\, v_F\, |\mathbf{q}| + O\left[\frac{|\mathbf{q}|^2}{|\mathbf{K}|^2}\right] \tag{4}$$

with $\mathbf{q}$ being the momentum of the crystal relative to a Dirac point. Each of these two regions is named a valley.

The above dispersion relationship (4) demonstrates that the electrons in a state of the band move at the speed

$$\mathbf{v}_{\pm} = \frac{1}{\hbar}\mathbf{grad}_{\mathbf{k}}E_{\pm} = \pm\frac{3}{2\hbar}at\frac{\mathbf{q}}{|\mathbf{q}|}. \tag{5}$$

The constant $\frac{3}{2\hbar}at = v_F$ is the *Fermi velocity* for the graphene and it has a value of about $v_F \approx \frac{c}{300}$, with c being the vacuum light speed. It is interesting to observe that, according to (5), the electrons in the conduction band move at the Fermi velocity in the direction of the momentum, while those of the valence band do so in the opposite direction. The dispersion relationship (4) has been observed experimentally [23] by means of the dependence of the cyclotronic mass of electrons on the electronic density in graphene. This relationship proves to be $m^* = \frac{\hbar}{v_F}\sqrt{\pi n}$, rather than a constant, as in the case of a parabolic dispersion relationship, and this has important consequences as regards the speed of electrons in both bands.

In contrast to what happens in conventional semiconductors, in which the dependence is quadratic in the momentum, in the case of graphene this dependence is linear, such that the carriers move at fixed speed in both bands, independent of the energy or the momentum, in the same direction as the momentum of the crystal in the case of the conduction band, and in the opposite direction in the valence band. This behavior resembles that of an ultrarelativistic particle described by a Dirac Hamiltonian [24], and hence this Hamiltonian can be used to describe the state of the carriers in two-dimensional graphene.

According to this new image, the two-dimensional electrons in a graphene sheet can be described by an effective Hamiltonian consisting of two copies of the two-dimensional Dirac Hamiltonian, one for momenta close to $\mathbf{K}$ and another for $\mathbf{K}'$. The wavefunctions for momenta close to $\mathbf{K}$ and $\mathbf{K}'$ are related by time-reversal symmetry [4, 24]. Therefore, only a single copy of the two-dimensional Dirac Hamiltonian is necessary, which, in the case of the existence of an external potential $V(x, y)$, can be expressed as

$$H = v_F(\sigma_x P_x + \sigma_y P_y) + V(x, y) \tag{6}$$

with σ_x and σ_y being the Dirac matrix

$$\sigma_x = \begin{pmatrix} 0 & 1 \\ 1 & 0 \end{pmatrix} \qquad \sigma_y = \begin{pmatrix} 0 & -\mathrm{i} \\ \mathrm{i} & 0 \end{pmatrix}.$$

Each electron in the graphene with a wave vector next to a Dirac point is described by a wavefunction of two spinorial components

$$\Psi(x, y, t) = \mathrm{e}^{-\mathrm{i}\frac{E}{\hbar}t}\begin{pmatrix} \varphi_1(x, y) \\ \varphi_2(x, y) \end{pmatrix} \tag{7}$$

fulfilling the system of coupled equations

$$E\varphi_1 = V\varphi_1 - \mathrm{i}\hbar\mathrm{v_F}\left(\frac{\partial\varphi_2}{\partial\mathrm{x}} - \mathrm{i}\frac{\partial\varphi_2}{\partial\mathrm{y}}\right) \tag{8}$$

$$E\varphi_2 = V\varphi_2 - \mathrm{i}\hbar\mathrm{v_F}\left(\frac{\partial\varphi_1}{\partial\mathrm{x}} + \mathrm{i}\frac{\partial\varphi_1}{\partial\mathrm{y}}\right). \tag{9}$$

For a free electron ($V = 0$) or one subjected to a constant potential energy $V = U_o \neq 0$, the solution is expressed as a linear combination of spinorial plane waves. The wavefunctions of the basis are classified by their momentum in the crystal (relative to a Dirac point) $\mathbf{k} = (k_x, k_y)$ and their energy. The accessible states for the electrons correspond to wavefunctions

$$\Psi_\pm(x, y, t) = \frac{1}{\sqrt{2LW}}\, \mathrm{e}^{\mathrm{i}\left(\mathbf{k}.\mathbf{r} - \frac{E_\pm}{\hbar}t\right)} \begin{pmatrix} 1 \\ \pm\frac{k_x + \mathrm{i}k_y}{|\mathbf{k}|} \end{pmatrix}, \tag{10}$$

which are normalized in the $L \times W$ rectangle, whose properties are

$$E_\pm = U_o \pm \hbar v_F |\mathbf{k}| \qquad \mathbf{v}_\pm = \frac{1}{\hbar}\mathbf{grad}_\mathbf{k} E_\pm = \pm v_F \frac{\mathbf{k}}{|\mathbf{k}|} \tag{11}$$

$$\hat{h}_\pm = \frac{1}{2}\frac{\Psi_\pm^\dagger \sigma.\mathbf{p}\Psi_\pm}{|\mathbf{p}|} = \pm\frac{1}{2} \qquad \mathbf{j}_\pm = -ev_F \Psi_\pm^\dagger \sigma \Psi_\pm = \mp e\frac{v_F}{LW}\frac{\mathbf{k}}{|\mathbf{k}|}. \tag{12}$$

These states form the conduction (case $(+)$) and valence (case $(-)$) bands in graphene subjected to a constant external potential. Their energy is shifted by a fixed quantity, U_o, with respect to free graphene. All electrons in the states $\Psi_\pm(x, y, t)$ have the same crystal momentum $\mathbf{k}$ and a definite helicity (the helicity operator $\hat{h} = \frac{1}{2}\frac{\sigma.\mathbf{p}}{|\mathbf{p}|}$), representing the pseudospin projection over the momentum. In these two cases, the helicity has a fixed value of $\pm\frac{1}{2}$. They all move at fixed Fermi velocity, regardless of their energy or momentum. It should be noted that electrons in $(+)$ states move in the same direction as their momentum, and those in $(-)$ states move in the opposite direction. In contrast, electrons in $(-)$ states carry current in the same direction as their momentum and those in $(+)$ states in the opposite direction.

It is worth mentioning that the serious problems occurring in the interpretation of negative energy electrons in the primitive Dirac theory no longer exist here. Indeed, the inconsistency stems from the fact that the existence of negative energy levels $E_- = -\hbar v_F |\mathbf{k}|$ and any momentum prevents the existence of a fundamental energy level. Now, however, within the graphene this situation no longer occurs, because the structure of the network imposes periodic boundary conditions, limiting the number of allowable moments, and turns them into a finite set. The proximity of existing levels allows us, however, to treat this set as continuous, even though in each band there are a finite number of states and a fundamental energy level.

Furthermore, the fact that the electric current carried by electrons from the valence band *seems* to be carried by a positively charged virtual particle allows us to introduce the concept of a *hole* to describe such a particle.

Our aim is to study the behavior of some electronic devices when a conventional semiconductor is replaced by a sheet of monolayer graphene.

We are particularly interested in studying the behavior of several different electronic devices (some field-effect transistors, FET, for example), which, through a suitable experimental setup and using different gate potentials, subject the graphene to external potentials that can be simulated in different ways. In the simplest approximation, we consider that this potential is comparable to one or two potential barriers, as in figure 1, and so below we attempt to obtain the corresponding *transmission coefficients*, because it has been known since the work of Landauer [25, 26] that the current coherent transport in these devices is determined by the *probability that an electron will be transmitted through them*.

3. A single-potential barrier

The energy barrier is described by the potential

$$V(x, y) = \begin{cases} 0 & x < a \\ U_o & a < x < a + L \\ 0 & a + L < x. \end{cases} \tag{13}$$

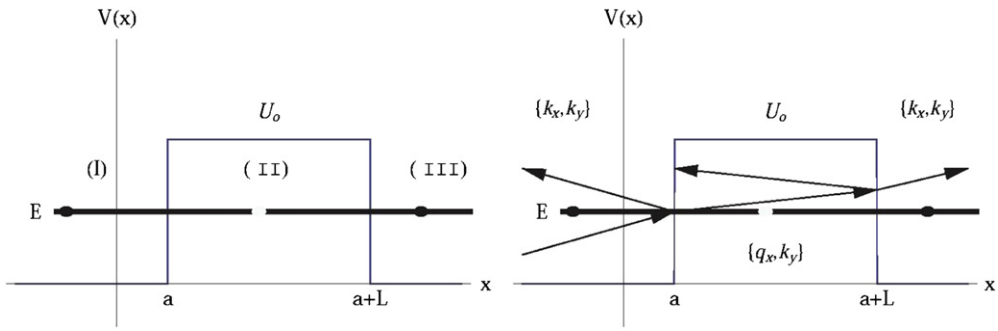

Figure 1. A potential barrier.

The barrier potential energy of $U_o = -eV_o$ is obtained in electronic devices with a gate potential V_o: negative when the carriers are negative, electrons, and positive for positive carriers, holes. The symmetry of the system could have been used and the barrier described as centered at the origin. We have chosen to displace it in order to apply the results to other more general cases.

In order to construct the admissible states in each region, certain aspects must be taken into account. Since the Hamiltonian is independent of time, the energy is a constant of motion, and all states must have the same fixed energy E. In the regions where the electron is free, regions (I) and (III), the modulus of the momentum must be $|\mathbf{k}| = \pm\frac{E}{\hbar v_F}$, depending on whether we consider the conduction or valence band. Inside the barrier, region (II), the momentum must be changed to $|\mathbf{q}| = \pm\frac{E-U_o}{\hbar v_F}$, depending on the sign$(E - U_o)$. This means that for a potential barrier ($U_o > 0$), in the region where the potential is null, the states with both positive and negative energies (in the conduction or valence band) can be propagated. Inside the barrier, on the other hand, we must consider several cases.

- When $E > U_o > 0$, there is only one physically acceptable value for $|\mathbf{q}|$. If we choose the positive sign in the equation, $|\mathbf{q}| = \pm\frac{E-U_o}{\hbar v_F}$, corresponding to a state of the conduction band. Thus, the electrons propagate in all regions across the conduction band.
- When $U_o > E > 0$, the negative sign must be chosen, corresponding to a given state of the valence band. In this case, the electrons propagating along the conduction band in the free region can only propagate in the barrier across the valence band.
- When $E < 0$, the electrons can only propagate along the valence band in all regions.

Since the potential does not depend on the coordinate y, the component k_y of the wave vector should be the same in all regions. In contrast, the component x, which can take the values $k_x = \pm\sqrt{\frac{E^2}{\hbar^2 v_F^2} - k_y^2}$ in regions (I) and (III), corresponding to incident and reflected waves, must change to $q_x = \pm\sqrt{\frac{(E-U_o)^2}{\hbar^2 v_F^2} - k_y^2}$ in region (II). In both cases, both k_x and q_x can be real or imaginary. In this latter case, the waves are evanescent. This behavior can be interpreted in terms of the well-known Snell reflection and refraction laws. The plane waves that carry the electron in each region must fulfil the following.

- The angle of incidence (formed between the incident ray and the normal to the interface) Φ is equal to the reflection angle Φ' (angle between the reflected ray and the normal to the interface).

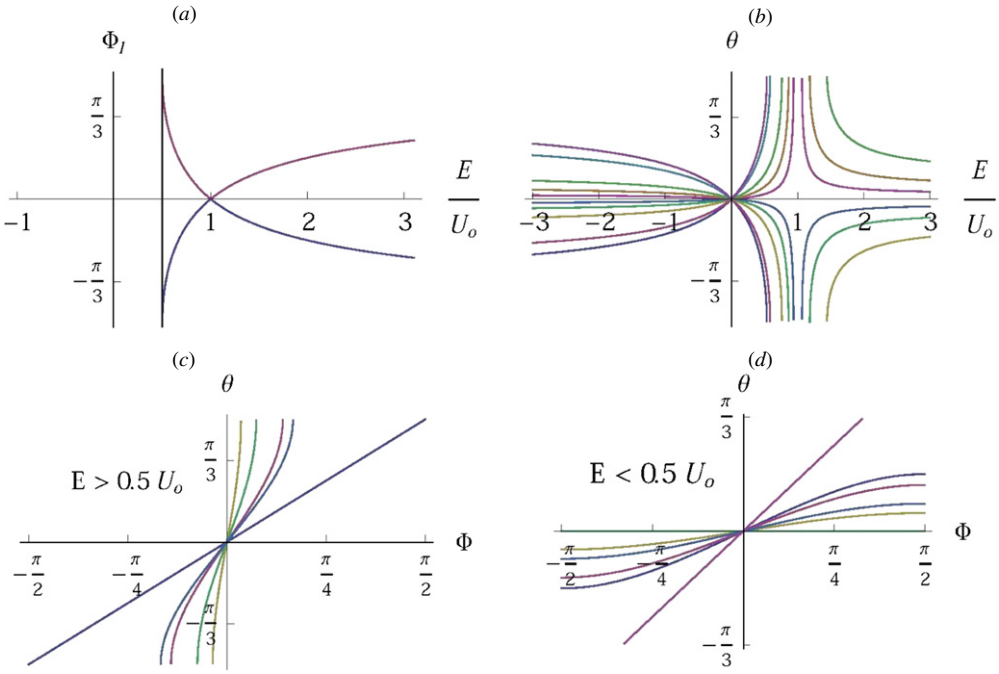

Figure 2. (*a*) Limit angle versus energy. (*b*) Transmission angles as a function of the energy for fixed values in the incidence angles. (*c*) and (*d*) Transmission angles as a function of the incidence angle for fixed values in the energy.

- The angle of incidence Φ and the transmission angle Θ (formed between the transmitted ray and the normal to the interface) must fulfil

$$k_y = |\mathbf{k}| \sin \Phi = |\mathbf{q}| \sin \Theta \tag{14}$$

$$|E| \sin \Phi = |E - U_o| \sin \Theta. \tag{15}$$

For certain energies, there is a limit incidence angle such that the particle is transmitted at 90°. For higher angles of incidence, the x component of the wave vector becomes imaginary. The incident plane waves become evanescent waves as they are being transmitted inside the barrier. These waves are described by real exponents. The *limit angle* is set by the condition

$$\Phi_l = \arcsin \left| 1 - \frac{U_o}{E} \right|. \tag{16}$$

Thus, electrons with an energy of less than 0.5 U_o cannot undergo total reflection at the barrier and are transmitted with a transmission angle lower than the incidence angle, i.e. they approach the normal direction.

Electrons with energy equal to 0.5 U_o are transmitted with a transmission angle equal to the incident angle, and the electrons with higher energy can only be transmitted by means of a plane wave if the angle of incidence is between the values $-\Phi_l$ and Φ_l corresponding to the value of their energy. When they do, they move away from the normal direction.

In particular, for the energy $E = U_o$, the limit angle is zero. Only for normal incidence can there be plane waves transmitting inside the barrier. This behavior is shown in figure 2.

Based on these considerations, we can construct the solution to our potential as

$$\Psi_{\mathrm{I}}(x,y,t)=\frac{\mathrm{e}^{\mathrm{i}\left(k_y y-\frac{E}{\hbar}t\right)}}{\sqrt{2LW}}\left\{\mathrm{e}^{\mathrm{i}k_x x}\begin{pmatrix}1\\ s\frac{k_x+\mathrm{i}k_y}{\sqrt{k_x^2+k_y^2}}\end{pmatrix}+r\mathrm{e}^{-\mathrm{i}k_x x}\begin{pmatrix}1\\ s\frac{-k_x+\mathrm{i}k_y}{\sqrt{k_x^2+k_y^2}}\end{pmatrix}\right\} \tag{17a}$$

$$\Psi_{\mathrm{II}}(x,y,t)=\frac{\mathrm{e}^{\mathrm{i}\left(k_y y-\frac{E}{\hbar}t\right)}}{\sqrt{2LW}}\left\{A\mathrm{e}^{\mathrm{i}q_x x}\begin{pmatrix}1\\ s_1\frac{q_x+\mathrm{i}k_y}{\sqrt{q_x^2+k_y^2}}\end{pmatrix}+B\mathrm{e}^{-\mathrm{i}q_x x}\begin{pmatrix}1\\ s_1\frac{-q_x+\mathrm{i}k_y}{\sqrt{q_x^2+k_y^2}}\end{pmatrix}\right\} \tag{17b}$$

$$\Psi_{\mathrm{III}}(x,y,t)=\frac{\mathrm{e}^{\mathrm{i}\left(k_y y-\frac{E}{\hbar}t\right)}}{\sqrt{2LW}}t\mathrm{e}^{\mathrm{i}k_x x}\begin{pmatrix}1\\ s\frac{k_x+\mathrm{i}k_y}{\sqrt{k_x^2+k_y^2}}\end{pmatrix}, \tag{17c}$$

where we have denoted $s=\mathrm{sign}(E)$ and $s_1=\mathrm{sign}(E-U_o)$, and it has been considered that the particles initially spreading from left to right can be reflected and transmitted, although in region (III), once past the barrier, there are only particles propagating to the right. It has also been assumed that the angle of incidence is less than the limit angle $\phi<\phi_l$.

In order to connect these functions at the boundaries, we should include the condition that the wavefunction must be continuous at the boundaries, such that the following must be fulfilled:

$$\Psi_{\mathrm{I}}(a,y,t)=\Psi_{\mathrm{II}}(a,y,t) \tag{18a}$$

$$\Psi_{\mathrm{II}}(a+L,y,t)=\Psi_{\mathrm{III}}(a+L,y,t). \tag{18b}$$

Note that, finally, the characterization of the electronic states requires a unique initial condition. Another procedure [27], which decouples the Dirac system and converts it into an equivalent Schrödinger equation system, has the disadvantage of needing the introduction of a second initial condition, which is spurious.

The unknown coefficients are

$$r=\frac{-\mathrm{e}^{\mathrm{i}2ak_x}k_y k_+(|\mathbf{k}|-ss_1|\mathbf{q}|)\sin(Lq_x)}{|\mathbf{k}|\left(k_x q_x\cos(Lq_x)+\mathrm{i}\left(k_y^2-ss_1|\mathbf{k}||\mathbf{q}|\right)\sin(Lq_x)\right)} \tag{19}$$

$$A=\frac{\mathrm{e}^{\mathrm{i}a(k_x-q_x)}\mathrm{e}^{-\mathrm{i}Lq_x}k_x(|\mathbf{k}|q_-+ss_1|\mathbf{q}|k_+)}{2|\mathbf{k}|\left(k_x q_x\cos(Lq_x)+\mathrm{i}\left(k_y^2-ss_1|\mathbf{k}||\mathbf{q}|\right)\sin(Lq_x)\right)} \tag{20}$$

$$B=\frac{\mathrm{e}^{\mathrm{i}a(k_x+q_x)}\mathrm{e}^{\mathrm{i}Lq_x}k_x(|\mathbf{k}|q_+-ss_1|\mathbf{q}|k_+)}{2|\mathbf{k}|(k_x q_x\cos(Lq_x)+\mathrm{i}\left(k_y^2-ss_1|\mathbf{k}||\mathbf{q}|\right)\sin(Lq_x))} \tag{21}$$

$$t=\frac{\mathrm{e}^{-\mathrm{i}k_x L}k_x q_x}{k_x q_x\cos(Lq_x)+\mathrm{i}\left(k_y^2-ss_1|\mathbf{k}||\mathbf{q}|\right)\sin(Lq_x)}. \tag{22}$$

In applications, we need to know mainly the reflection and transmission coefficients in a given direction, i.e. in our case the direction x . These coefficients are defined by the ratio between two probability currents: the reflected and incident currents, $-\frac{\Psi^+_{\mathrm{ref}}\sigma_x\Psi_{\mathrm{ref}}}{\Psi^+_{\mathrm{inc}}\sigma_x\Psi_{\mathrm{inc}}}$, and the transmitted and incident currents, $\frac{\Psi^+_{\mathrm{trans}}\sigma_x\Psi_{\mathrm{trans}}}{\Psi^+_{\mathrm{inc}}\sigma_x\Psi_{\mathrm{inc}}}$. In our system, these are

$$R=rr^*=\frac{k_y^2(|\mathbf{q}|-ss_1|\mathbf{k}|)^2\sin^2(Lq_x)}{k_x^2q_x^2\cos^2(Lq_x)+\left(k_y^2-ss_1|\mathbf{k}||\mathbf{q}|\right)^2\sin^2(Lq_x)} \tag{23}$$

$$T=tt^*=\frac{k_x^2q_x^2}{k_x^2q_x^2\cos^2(Lq_x)+\left(k_y^2-ss_1|\mathbf{k}||\mathbf{q}|\right)^2\sin^2(Lq_x)}. \tag{24}$$

Naturally, $R+T=1$ and they are symmetric: $T(\phi)=T(-\phi)$. The transmission coefficient obtained coincides with that described in [4] and reflects some already known behavior.

The barrier is transparent for all the electrons impinging perpendicularly to it, whatever their energy [7]. This phenomenon, called the Klein paradox [9], does not occur for non-relativistic electrons, for which the transmission coefficient at normal incidence is always less than 1. The barrier is also transparent for those electrons with $q_x = \frac{n\pi}{L}$, i.e. those whose energy and angle of incidence are

$$n^2 \frac{\pi^2 \hbar^2 v_F^2}{L^2} = (E - U_o)^2 - E^2 \sin^2 \phi. \tag{25}$$

Up to here, it has been considered that the electrons impinge on the barrier with an angle smaller than the limit angle. If they do so with a greater angle, the analysis is still valid; we must merely change, in the above formulae, q_x for $\mathrm{i}q_x$, which transforms the plane waves $\mathrm{e}^{\pm \mathrm{i} q_x x}$ into evanescent waves $\mathrm{e}^{\mp q_x x}$. Inside the barrier, the electron wavefunction does not contain oscillatory but exponential terms. Regarding the coefficients, we have to replace $\cos(Lq_x)$ by $\cosh(Lq_x)$ and $\sin(Lq_x)$ by $\mathrm{i}\sinh(Lq_x)$. In particular, in this case, the transmission coefficient is

$$T = \frac{k_x^2 q_x^2}{k_x^2 q_x^2 \cosh^2(Lq_x) + \left(k_y^2 - s s_1 |\mathbf{k}||\mathbf{q}|\right)^2 \sinh^2(Lq_x)}. \tag{26}$$

In order to analyze the transport properties, it is interesting to express this coefficient in terms of the energy, the height and the length of the barrier and the angle of incidence. In particular, we obtain

- if $\phi \leqslant \phi_l$,

$$T = \frac{1}{1 + \tan^2 \phi \dfrac{\sin^2 \left\{ \frac{LU_o}{\hbar v_F} \sqrt{\left(\frac{E}{U_o} - 1\right)^2 - \left(\frac{E}{U_o}\right)^2 \sin^2 \phi} \right\}}{\left(\frac{E}{U_o} - 1\right)^2 - \left(\frac{E}{U_o}\right)^2 \sin^2 \phi}}; \tag{27}$$

- if $\phi \geqslant \phi_l$,

$$T = \frac{1}{1 + \tan^2 \phi \dfrac{\sinh^2 \left\{ \frac{LU_o}{\hbar v_F} \sqrt{\left(\frac{E}{U_o}\right)^2 \sin^2 \phi - \left(\frac{E}{U_o} - 1\right)^2} \right\}}{\left(\frac{E}{U_o}\right)^2 \sin^2 \phi - \left(\frac{E}{U_o} - 1\right)^2}}. \tag{28}$$

These values (which are exact) are reduced, for high values of the energy of incident electrons, to the approximate values considered in [4]. However, it should be noted that the difference between the two expressions can be significant if $E \approx V_o$.

Note that the transmission coefficient only depends on three variables: the relative energy $\frac{E}{U_o}$, the product LU_o and the angle of incidence. A graphic representation of some of these values is shown in figures 3 and 4. The factor LU_o is expressed in eV nm.

Figure 3 shows that for a fixed energy, the transmission coefficient tends to decrease more or less steeply as the angle of incidence increases. When the product LU_o is large enough, the resonances described in formula (25) begin to appear. It may also be observed that the values of energy, $\frac{E}{U_o} < 0.5$, are transmitted without decaying abruptly, whatever the angle of incidence. When, on the other hand, $\frac{E}{U_o} > 0.5$, the existence of an energy-dependent limit angle is evident.

Figure 4 shows that for a fixed incidence angle, the transmission coefficient is symmetric about the axis $E = U_o \cos^{-2} \phi$. This means that the states in the valence band with energy $E = (\cos^{-2} \phi - \xi) U_o$ and those in the conduction band with energy $E = (\cos^{-2} \phi + \xi) U_o$ are transmitted with the same probability. Moreover, this coefficient drops to almost zero between

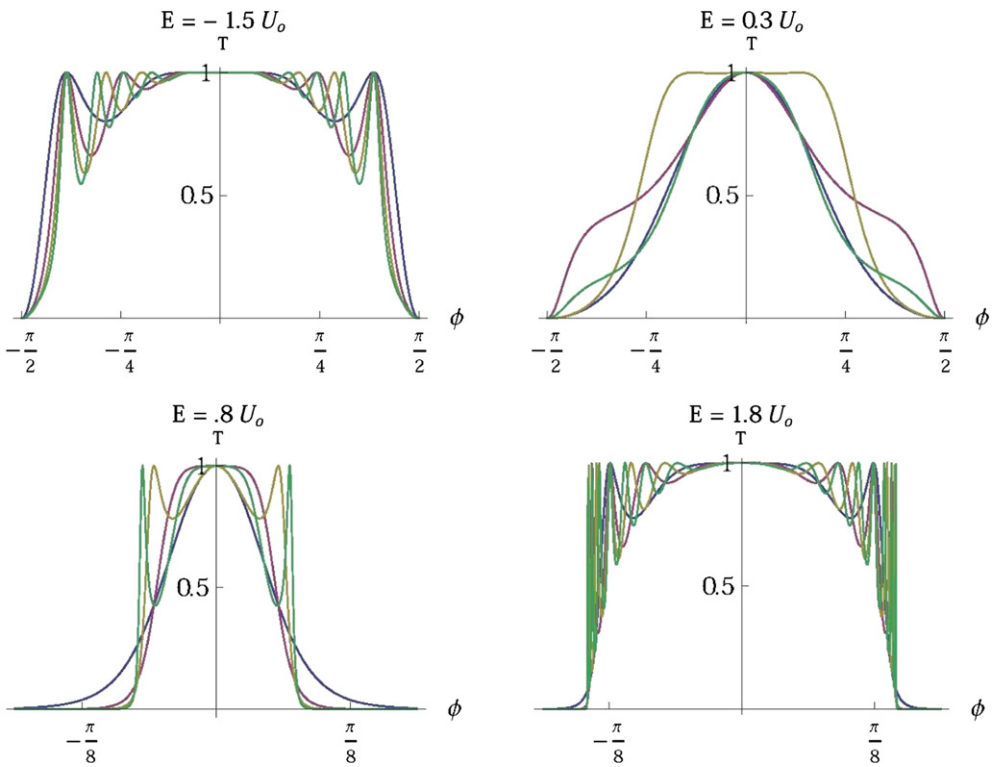

Figure 3. Transmission coefficient as a function of the incidence angle for some values of the energy. The different curves correspond to LU_o = 5, 10, 15 and 20 eV nm.

the energy values $(1 + \sin\phi)^{-1}U_o$ and $(1 - \sin\phi)^{-1}U_o$, for which the angle of incidence exceeds the limit angle and electron transmission occurs via evanescent waves. In practice, an energy gap of $2U_o \sin|\phi| \cos^{-2}\phi$ appears around the axis of symmetry. For the energies in the gap, the probability of transmitting an electron is almost zero.

Since in many experiments the height of the potential barrier is controlled through a gate potential, it is interesting to see how the system behaves for different values of this height which, ultimately, is easily tunable. In figure 5, several contour lines of the transmission coefficient are represented for different values of the height U_o and length L of the barrier for fixed energy and angle of incidence values .

The case of a potential well $U_o < 0$ can also be treated similarly. Essentially, the same results are found. The coefficients r, A, B and t are formally the same as those found in the case of the barrier. In particular, the transmission coefficient T is identical to (26). The only difference is the negative value of U_o. Note that the transmission coefficient satisfies $T(E, U_o) = T(-E, -U_o)$, which, applied to the electrons in graphene, means that the probability of transmission of an electron in the conduction band through a barrier with a given height is the same as that of an electron from the valence band with the opposite energy through a well whose depth is equal to the height of the barrier. As a result, the electrical conduction properties of n- or p-doped graphene are identical, except for the sign of the carriers.

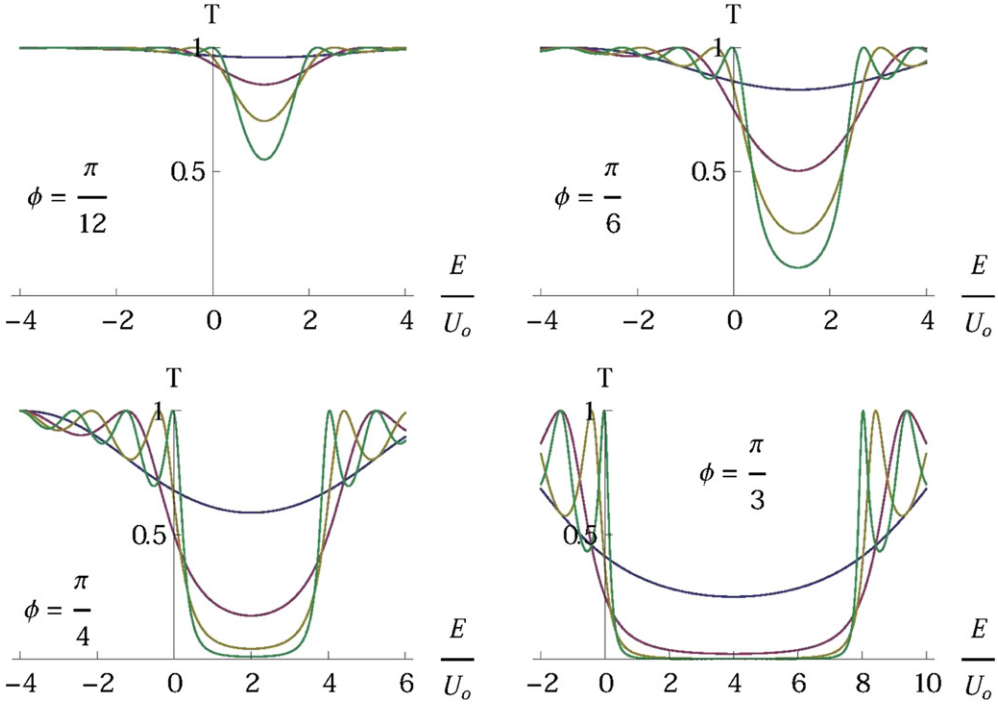

Figure 4. Transmission coefficient as a function of the energy for some fixed incidence angles. The different curves correspond to $LU_o = 0.5$, 1, 1.5 and 2 eV nm.

4. Two-potential barriers

We now consider two-potential barriers, as in figure 6. These barriers, which are separated by a certain distance, may be different in height and length. They are described by

$$V(x,y) = \begin{cases} 0 & x < a \\ U_1 & a < x < a + L_1 \\ 0 & a + L_1 < x < a + L_1 + D \\ U_2 & a + L_1 + D < x < a + L_1 + D + L_2 \\ 0 & a + L_1 + D + L_2 < x. \end{cases} \tag{29}$$

This system is essentially an extension of the previous one. We can build the solution for this new potential as

$$\Psi_{\mathrm{I}}(x,y,t) = \frac{\mathrm{e}^{\mathrm{i}\left(k_y y - \frac{E}{\hbar}t\right)}}{\sqrt{2LW}} \left\{ \mathrm{e}^{\mathrm{i}k_x x} \begin{pmatrix} 1 \\ s\frac{k_x + \mathrm{i}k_y}{\sqrt{k_x^2 + k_y^2}} \end{pmatrix} + r\mathrm{e}^{-\mathrm{i}k_x x} \begin{pmatrix} 1 \\ s\frac{-k_x + \mathrm{i}k_y}{\sqrt{k_x^2 + k_y^2}} \end{pmatrix} \right\} \tag{30a}$$

$$\Psi_{\mathrm{II}}(x,y,t) = \frac{\mathrm{e}^{\mathrm{i}\left(k_y y - \frac{E}{\hbar}t\right)}}{\sqrt{2LW}} \left\{ A_1\, \mathrm{e}^{q_{1x}x} \begin{pmatrix} 1 \\ s_1\frac{q_{1x} + \mathrm{i}k_y}{\sqrt{q_{1x}^2 + k_y^2}} \end{pmatrix} + B_1\, \mathrm{e}^{-\mathrm{i}q_{1x}x} \begin{pmatrix} 1 \\ s_1\frac{-q_{1x} + \mathrm{i}k_y}{\sqrt{q_{1x}^2 + k_y^2}} \end{pmatrix} \right\} \tag{30b}$$

$$\Psi_{\mathrm{III}}(x,y,t) = \frac{\mathrm{e}^{\mathrm{i}\left(k_y y - \frac{E}{\hbar}t\right)}}{\sqrt{2LW}} \left\{ C_1\, \mathrm{e}^{\mathrm{i}k_x x} \begin{pmatrix} 1 \\ s\frac{k_x + \mathrm{i}k_y}{\sqrt{k_x^2 + k_y^2}} \end{pmatrix} + D_1\, \mathrm{e}^{-\mathrm{i}k_x x} \begin{pmatrix} 1 \\ s\frac{-k_x + \mathrm{i}k_y}{\sqrt{k_x^2 + k_y^2}} \end{pmatrix} \right\} \tag{30c}$$

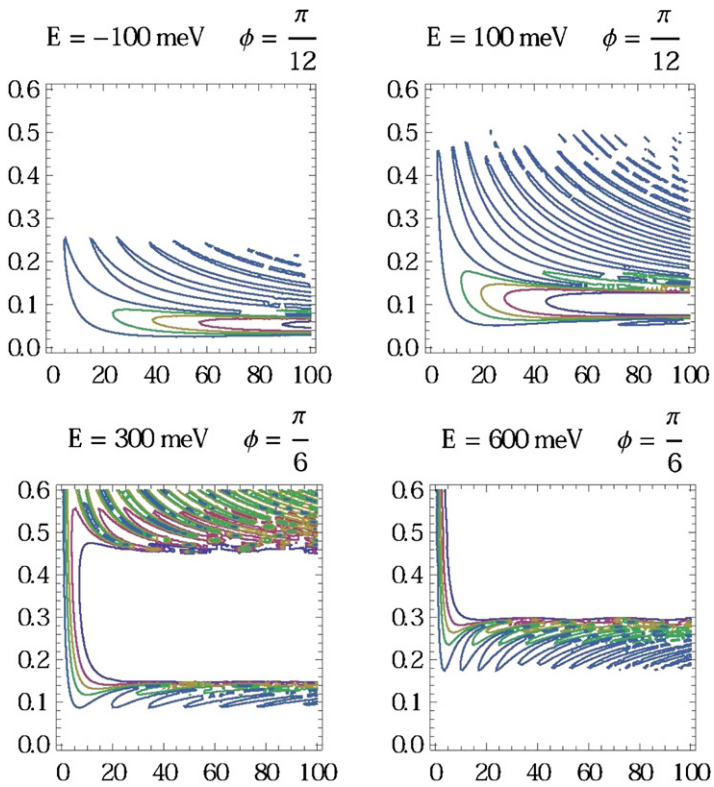

Figure 5. Contour lines for T= 0.1, 0.3, 0.5, 0.7 and 0.9. L (nm) are represented on the horizontal axis and U_o (eV) on the vertical one.

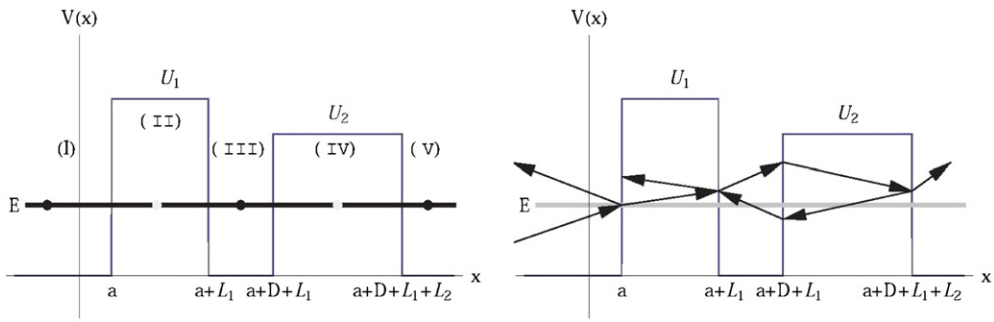

Figure 6. A double-potential barrier.

$$\Psi_{\mathrm{IV}}(x,y,t) = \frac{\mathrm{e}^{\mathrm{i}\left(k_y y - \frac{E}{\hbar}t\right)}}{\sqrt{2LW}}\left\{A_2\,\mathrm{e}^{q_{2_x}x}\begin{pmatrix}1\\ s_2\frac{q_{2_x}+\mathrm{i}k_y}{\sqrt{q_{2_x}^2+k_y^2}}\end{pmatrix} + B_2\,\mathrm{e}^{-q_{2_x}x}\begin{pmatrix}1\\ s_2\frac{-q_{2_x}+\mathrm{i}k_y}{\sqrt{q_{2_x}^2+k_y^2}}\end{pmatrix}\right\} \tag{30d}$$

$$\Psi_{\mathrm{V}}(x,y,t) = \frac{\mathrm{e}^{\mathrm{i}\left(k_y y - \frac{E}{\hbar}t\right)}}{\sqrt{2LW}}t\,\mathrm{e}^{\mathrm{i}k_x x}\begin{pmatrix}1\\ s\frac{k_x+\mathrm{i}k_y}{\sqrt{k_x^2+k_y^2}}\end{pmatrix}, \tag{30e}$$

where the sign $s = \mathrm{sign}(E)$ distinguishes the states in the conduction band from those in the valence band in the vacuum. Likewise, the sign $s_i = \mathrm{sign}(E - U_i)$ plays the same role inside the barriers. As in the case of a single barrier, it is considered that the particles are initially moving from left to right and that they can be reflected and transmitted, but in region (V), once all barriers have been crossed, there are only particles propagating to the right. Again, the energy E and the momentum component k_y of the electron are conserved. The momentum component k_x is adjusted in each region to $\pm k_x$ in the vacuum and $\pm q_{i_x}$ in each of the barriers. The reflection and transmission properties seen in the case of a single barrier are also satisfied in each of the interfaces of the problem, with the addition that there are now *two limit angles* distinguishing propagation in the form of plane waves from evanescent ones. These two *limit* angles are

$$\Phi_i^l = \arcsin\left|1 - \frac{U_i}{E}\right| \qquad i = 1, 2. \tag{31}$$

The boundary conditions are now

$$\Psi_{\mathrm{I}}(a, y, t) = \Psi_{\mathrm{II}}(a, y, t) \tag{32a}$$

$$\Psi_{\mathrm{II}}(a + L_1, y, t) = \Psi_{\mathrm{III}}(a + L_1, y, t) \tag{32b}$$

$$\Psi_{\mathrm{III}}(a + L_1 + D, y, t) = \Psi_{\mathrm{IV}}(a + L_1 + D, y, t) \tag{32c}$$

$$\Psi_{\mathrm{IV}}(a + L_1 + D + L_2, y, t) = \Psi_{\mathrm{V}}(a + L_1 + D + L_2, y, t) \tag{32d}$$

yielding

$$\begin{aligned} r = \frac{\pm \mathrm{e}^{\mathrm{i}2ak_x} k_y k_+}{|\mathbf{k}|(Z_1 + \mathrm{i}Z_2)} &\{(k_x q_{2_x} \cos \Xi_2 + \mathrm{i}G_2 \sin \Xi_2)(s_1|\mathbf{q_1}| - s|\mathbf{k}|) \sin \Xi_1 \\ &+ \mathrm{e}^{\mathrm{i}2Dk_x}(k_x q_{1_x} \cos \Xi_1 - \mathrm{i}G_1 \sin \Xi_1)(s_2|\mathbf{q_2}| - s|\mathbf{k}|) \sin \Xi_2\} \end{aligned} \tag{33}$$

$$\begin{aligned} A_1 = \pm \frac{\mathrm{e}^{\mathrm{i}a(k_x - q_{1_x}) - \mathrm{i}L_1 q_{1_x}} k_x}{2|\mathbf{k}|(Z_1 + \mathrm{i}Z_2)} &\{(s_1|\mathbf{q_1}|k_- - s|\mathbf{k}|q_{1_-})(k_x q_{2_x} \cos \Xi_2 + \mathrm{i}G_2 \sin \Xi_2) \\ &+ \mathrm{e}^{2\mathrm{i}Dk_x} k_y (k_+ q_{1_-} - s s_1 |\mathbf{k}||\mathbf{q_1}|)\,(s|\mathbf{k}| + s_2|\mathbf{q_2}|) \sin \Xi_2\} \end{aligned} \tag{34}$$

$$\begin{aligned} B_1 = -s \frac{\mathrm{e}^{\mathrm{i}a(k_x + q_{1_x}) + \mathrm{i}L_1 q_{1_x}} k_x}{2|\mathbf{k}|(Z_1 + \mathrm{i}Z_2)} &\{(s_1|\mathbf{q_1}|k_+ - s|\mathbf{k}|q_{1_+})(k_x q_{2_x} \cos \Xi_2 + \mathrm{i}G_2 \sin \Xi_2) \\ &+ \mathrm{e}^{2\mathrm{i}Dk_x} k_y (k_+ q_{1_+} + s s_1 |\mathbf{k}||\mathbf{q_1}|)(s|\mathbf{k}| - s_2|\mathbf{q_2}|) \sin \Xi_2\} \end{aligned} \tag{35}$$

$$C_1 = \mathrm{e}^{-\mathrm{i}L_1 k_x} k_x q_{1_x} \frac{k_x q_{2_x} \cos \Xi_2 + \mathrm{i}G_2 \sin \Xi_2}{Z_1 + \mathrm{i}Z_2} \tag{36}$$

$$D_1 = -s\mathrm{e}^{\mathrm{i}(2a + 2D + L_1)k_x} k_x k_y k_+ q_{1_x} \frac{(s|\mathbf{k}| - s_2|\mathbf{q_2}|)}{|\mathbf{k}|(Z_1 + \mathrm{i}Z_2)} \sin \Xi_2 \tag{37}$$

$$A_2 = s\mathrm{e}^{-\mathrm{i}(L_1 + L_2)q_{2_x}} \mathrm{e}^{\mathrm{i}(a+D)(k_x - q_{2_x})} k_x^2 q_{1_x} \frac{s|\mathbf{k}|q_{2_-} + s_2|\mathbf{q_2}|k_+}{2|\mathbf{k}|(Z_1 + \mathrm{i}Z_2)} \tag{38}$$

$$B_2 = s\mathrm{e}^{\mathrm{i}(L_1 + L_2)q_{2_x}} \mathrm{e}^{\mathrm{i}(a+D)(k_x + q_{2_x})} k_x^2 q_{1_x} \frac{s|\mathbf{k}|q_{2_+} - s_2|\mathbf{q_2}|k_+}{2|\mathbf{k}|(Z_1 + \mathrm{i}Z_2)} \tag{39}$$

$$t = \mathrm{e}^{-\mathrm{i}k_x(L_1+L_2)}\frac{k_x^2 q_{1_x} q_{2_x}}{Z_1 + \mathrm{i}Z_2}, \tag{40}$$

where G_1, G_2 ,Ξ_1, Ξ_2, Z_1 and Z_2 are

$$G_i = (k_y^2 - ss_i|\mathbf{k}||\mathbf{q_i}|), \qquad i = 1, 2, \tag{41}$$

$$\Xi_i = L_i q_{i_x}, \qquad i = 1, 2, \tag{42}$$

$$\begin{aligned} Z_1 = {} & k_y^2(s|\mathbf{k}| - s_1|\mathbf{q_1}|)(s|\mathbf{k}| - s_2|\mathbf{q_2}|)\cos(2Dk_x)\sin\Xi_1\sin\Xi_2 \\ & \times k_x^2 q_{1_x} q_{2_x}\cos\Xi_1\cos\Xi_2 - G_1G_2\sin\Xi_1\sin\Xi_2 \end{aligned} \tag{43}$$

$$\begin{aligned} Z_2 = {} & k_y^2(s|\mathbf{k}| - s_1|\mathbf{q_1}|)(s|\mathbf{k}| - s_2|\mathbf{q_2}|)\sin(2Dk_x)\sin\Xi_1\sin\Xi_2 \\ & + k_x(q_{2_x}G_1\cos\Xi_2\sin\Xi_1 + q_{1_x}G_2\cos\Xi_1\sin\Xi_2). \end{aligned} \tag{44}$$

Thinking about applications, we are principally interested in the reflection and transmission coefficients, which prove to be

$$T = 1 - R = tt^* = \frac{k_x^4 q_{1_x}^2 q_{2_x}^2}{Z_1^2 + Z_2^2}. \tag{45}$$

They also highlight the phenomenon of coupling between the two barriers due to the non-trivial appearance of the parameter D. If we consider that the two barriers are very separated, then the oscillations $\sin(2k_xD)$ and $\cos(2k_xD)$ are very fast and can be replaced by their mean value, zero. Under these conditions, the coupling between barriers disappears and the transmission coefficient is reduced to the product of coefficients of two independent barriers as one would expect in any Fabry–Perot-like device: $T = T_1 \cdot T_2$.

Also in this case, $T(\phi) = T(-\phi)$ and it is unity for a zero-incidence angle. The double barrier is transparent for all the electrons impinging perpendicularly to it, whatever its energy, and it is equally transparent to electrons with $q_{1_x} = \frac{n_1\pi}{L_1}$ and $q_{2_x} = \frac{n_2\pi}{L_2}$, i.e. the electrons whose energy and angle of incidence satisfy the dual condition

$$n_i^2\frac{\pi^2\hbar^2 v_F^2}{L_i^2} = (E - U_i)^2 - E^2\sin^2\phi, \qquad i = 1, 2. \tag{46}$$

As in the case of a single barrier, it is considered that the incident electrons coincide with an angle lower than the lowest of the two limit angles in the system (31). If they do so with an angle greater than either of them, the analysis is still valid and we simply have to replace q_{i_x} by $\mathrm{i}q_{i_x}$, which transforms the plane waves into evanescent waves. Inside one or both barriers, the electron transport does not contain oscillatory but exponential terms. Regarding the coefficients, it is necessary to replace $\cos(L_iq_{i_x})$ by $\cosh(L_iq_{i_x})$ and $\sin(L_iq_{i_x})$ by $\mathrm{i}\sinh(L_iq_{i_x})$.

Explicitly, the transmission coefficient of a double-potential barrier, expressed as a function of the characteristic parameters of the barrier (height, length and separation) and of the incident electron variables (energy and angle of incidence), is

$$T = \frac{1}{\hat{Z}_1^2 + \hat{Z}_2^2} \tag{47}$$

$$\begin{aligned} \hat{Z}_1 = {} & \cos\left(\frac{L_1\epsilon_1}{\hbar v_F}\right)\cos\left(\frac{L_2\epsilon_2}{\hbar v_F}\right) - \left(2U_1U_2\tan^2\Phi\sin^2\left(\frac{D\epsilon}{\hbar v_F}\right) + (E - U_1)(E - U_2)\right. \\ & \left. - E^2\sin\Phi^2\right)\frac{\sin\left(\frac{L_1\epsilon_1}{\hbar v_F}\right)}{\epsilon_1}\frac{\sin\left(\frac{L_2\epsilon_2}{\hbar v_F}\right)}{\epsilon_2} \end{aligned} \tag{48}$$

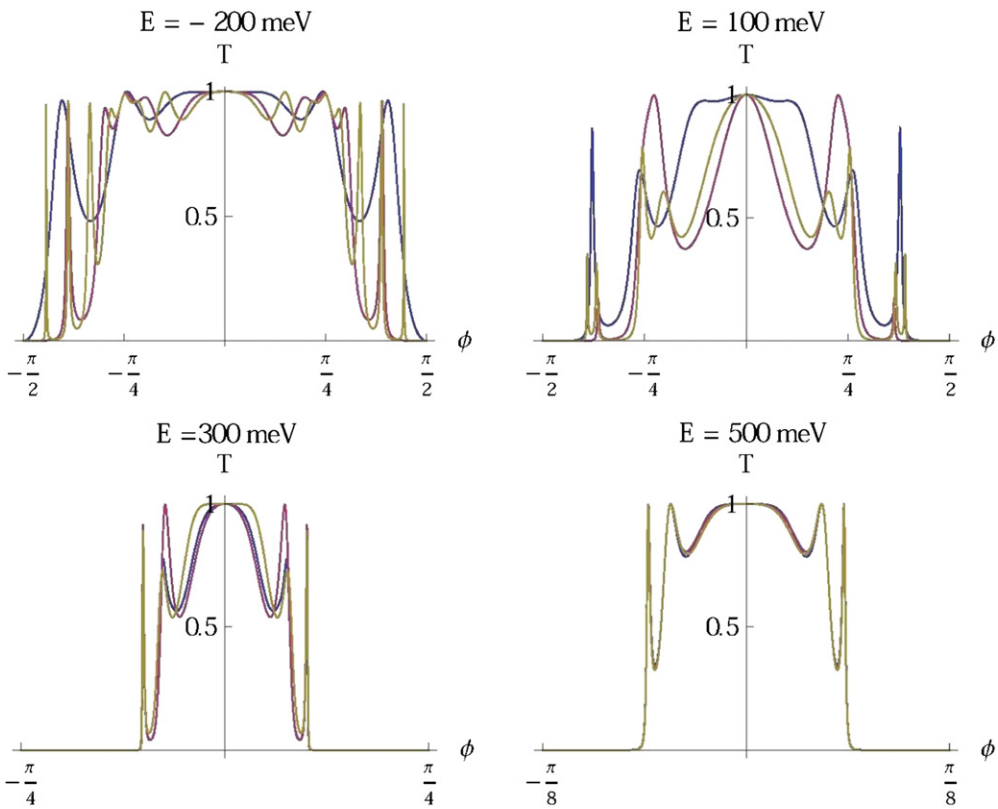

Figure 7. Transmission coefficient as a function of the incidence angle for some energy values. The curves correspond to $D = 0$, 20, 40 and 60 nm.

$$\hat{Z}_2 = \frac{U_1 - E\cos^2\Phi}{\cos\Phi}\cos\left(\frac{L_2\epsilon_2}{\hbar v_F}\right)\frac{\sin\left(\frac{L_1\epsilon_1}{\hbar v_F}\right)}{\epsilon_1} + \frac{U_2 - E\cos^2\Phi}{\cos\Phi}\cos\left(\frac{L_1\epsilon_1}{\hbar v_F}\right)\frac{\sin\left(\frac{L_2\epsilon_2}{\hbar v_F}\right)}{\epsilon_2} + U_1U_2\tan^2\Phi\sin\left(\frac{2D\epsilon}{\hbar v_F}\right)\frac{\sin\left(\frac{L_1\epsilon_1}{\hbar v_F}\right)}{\epsilon_1}\frac{\sin\left(\frac{L_2\epsilon_2}{\hbar v_F}\right)}{\epsilon_2} \tag{49}$$

$$\epsilon = E\cos\Phi \tag{50}$$

$$\epsilon_i = \sqrt{(E - U_i)^2 - E^2\sin^2\Phi}, \qquad i = 1, 2, \tag{51}$$

which is represented in figures 7 and 8 for the values $L_1 = 50$ nm, $L_2 = 60$ nm, $U_1 = 200$ meV and $U_2 = 400$ meV. These orders of magnitude are usually considered in the current bibliography [9, 18, 20]. In figure 7, it can be appreciated that for a fixed energy, the transmission coefficient envelope tends to decrease more or less steeply as the angle of incidence increases. The existence of a limit angle depending on the energy is evident.

Figure 8 shows that, for a fixed incidence angle, the transmission coefficient falls to almost zero for energy values between $(1 + \sin\phi)^{-1}U_1$ and $(1 - \sin\phi)^{-1}U_1$, is recovered in some cases and falls back between energy values of $(1 + \sin\phi)^{-1}U_2$ and $(1 - \sin\phi)^{-1}U_2$. In these

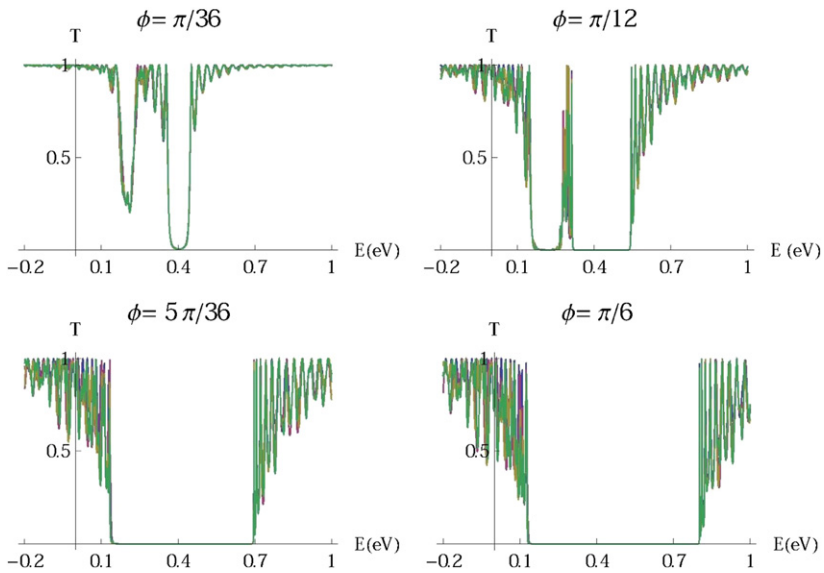

Figure 8. Transmission coefficient as a function of the energy for some incidence angles. The curves correspond to D = 0, 20, 40 and 60 nm.

intervals, the angle of incidence is greater than the limit angle and the transmission of electrons occurs through evanescent waves at one of the barriers. This is the case in figure 8 for $\phi = \frac{\pi}{36}$ and $\phi = \frac{\pi}{12}$. For $\phi > 0$, if $(1 - \sin\phi)^{-1}U_1 < (1 + \sin\phi)^{-1}U_2$, then in the energy spectrum two clearly defined regions where the transmission coefficient falls practically to zero can be distinguished. If $(1 - \sin\phi)^{-1}U_1 > (1 + \sin\phi)^{-1}U_2$, both regions are converted into a single one. This is the case in figure 8 for $\phi = \frac{5\pi}{36}$ and $\phi = \frac{\pi}{6}$. Note also in this case the existence of effective energy gaps within which the probability of transmission electron drops to practically zero.

Since the potential energy of the barrier is tunable by the gate potential in the experiments, we are again interested in seeing the changes that occur in the transmission as a function of the gate potentials. In figure 9, there are some lines of levels as a function of the potential U_1 on the horizontal axes and U_2 on the vertical axes for $L_1 =$ 50 nm, $L_2 =$ 60 nm and $D =$ 20 nm.

5. On the current and the conductance

In order to quantify the electric current across a certain device (the FET transistor, which has been mentioned above) when it is subjected to a V_{DS} bias, we now have to consider the transport of the carriers through the device and build the device characteristic, the current–voltage relationship. According to the Landauer formalism [28], the active conduction channel, the sheet of graphene under different gate potentials, is connected to two ideal reservoirs, the source and the drain, which yield electrons with several energies and different momenta.

In a system at equilibrium, the distribution of these electrons is given by the Fermi function [29]. When the device is polarized, this situation of equilibrium no longer occurs. However, if the bias applied is not too large, we can consider two different quasi-Fermi levels [28], one for each reservoir.

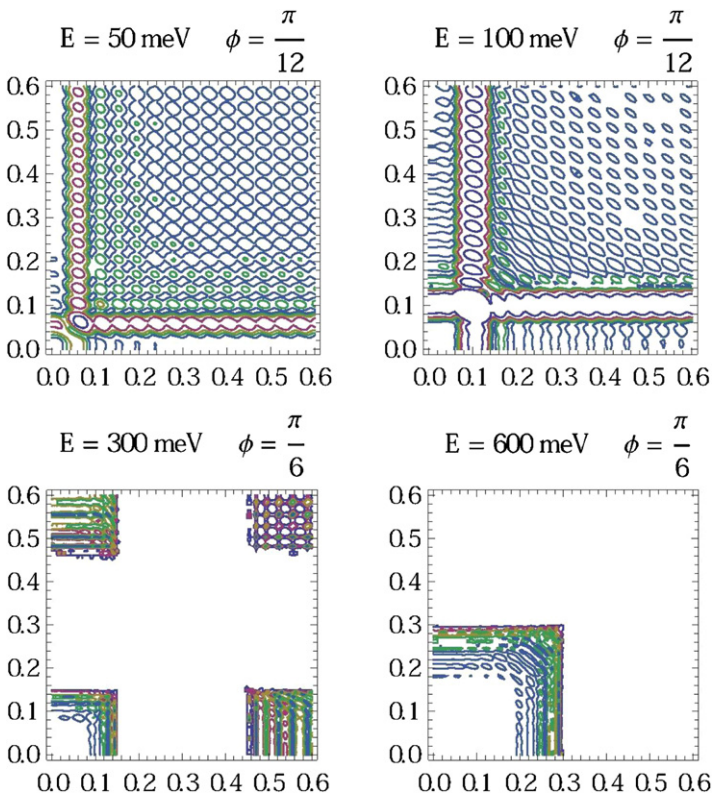

Figure 9. Contour lines for T= 0.1, 0.3, 0.5, 0.7 and 0.9. U_1 (eV) is represented on the horizontal axes and U_2 (eV) on the vertical ones.

The source, on the left side, provides an electron collective with input wave vectors $\mathbf{k} = (\mathbf{k}_x, \mathbf{k}_y)$, in thermodynamic equilibrium with an electrochemical potential μ_L. Similarly, the drain, on the right side, supplies electrons to another different electrochemical potential μ_R. The conventional electric current, which is established in the channel, is precisely due to these two electronic fluxes.

Each electron in the channel, in a state ψ, carries an electric current proportional to the probability flux given by

$$j_x^o = -ev_F \Psi^+ \sigma_x \Psi = -se\frac{v_F}{LW} T(E, \phi)\frac{k_x}{|\mathbf{k}|} = -se\frac{v_F}{LW} T(E, \phi)\cos\phi \tag{52}$$

with a dimension of *current intensity per length unity*. The total current is due to the current carried by all the electrons with all possible values of k_x and k_y. They enter the system from the reservoirs and propagate along the available orbitals. Their number, with momenta between (k_x, k_y) and $(k_x + \mathrm{d}k_x, k_y + \mathrm{d}k_y)$, depends on the number of available states and their degree of occupancy. It is known that each allowed momentum occupies a surface in the momentum space of the bi-dimensional graphene $\frac{2\pi}{L} \times \frac{2\pi}{W}$, and hence their number in the rectangle $\mathrm{d}k_x \mathrm{d}k_y$ is $2 \times 2 \times \frac{\mathrm{d}k_x \mathrm{d}k_y}{\frac{2\pi}{L} \times \frac{2\pi}{W}} = \frac{LW}{\pi^2} \mathrm{d}k_x\, \mathrm{d}k_y$ (2 due to the spin and 2 due to the duplicity of the Dirac valleys).

The electron number in this interval, since they are in equilibrium at a Fermi potential μ with an occupancy factor of $f_o(E,\mu) = \left(1+\exp\left\{\frac{E-\mu}{k_BT}\right\}\right)^{-1}$, is

$$\mathrm{d}n_{\mathrm{elec}} = 2\times 2\times LW\frac{\mathrm{d}k_x\,\mathrm{d}k_y}{4\pi^2}f_o(E,\mu) = \frac{LW}{\pi^2}f_o(E,\mu)\,\mathrm{d}k_x\,\mathrm{d}k_y \tag{53}$$

and, changing the coordinate system $\mathrm{d}k_x\mathrm{d}k_y = |\mathbf{k}|\mathrm{d}|\mathbf{k}|\mathrm{d}\phi$ and introducing the dispersion relationship $E = s\hbar v_F|\mathbf{k}|$, we have

$$\mathrm{d}n_{\mathrm{elec}} = s\times 2\times 2\times LW\frac{E\,\mathrm{d}E\,\mathrm{d}\phi}{h^2v_F^2}f_o(E,\mu). \tag{54}$$

The current density provided by these electrons is

$$\mathrm{d}j_x = -\frac{4e}{h^2v_F}T(E,\phi)f_o(E,\phi)\cos\phi E\,\mathrm{d}E\,\mathrm{d}\phi \tag{55}$$

and the total current density due to all electrons with all possible energies and angles of incidence is

$$j_x = \frac{I}{W} = -\frac{4e}{h^2v_F}\int_{-\frac{\pi}{2}}^{\frac{\pi}{2}}\cos\phi\,\mathrm{d}\phi\int_{-\infty}^{\infty}T(E,\phi)f_o(E,\mu)E\,\mathrm{d}E. \tag{56}$$

It must now be recalled that we have two contacts. Both of them compete in order to carry the channel to equilibrium with an electrochemical potential μ_L, the source, and μ_R, the drain. As a result, the current flows along the conduction channel; thus

$$j_x = -\frac{4e}{h^2v_F}\int_{-\frac{\pi}{2}}^{\frac{\pi}{2}}\cos\phi\,\mathrm{d}\phi\int_{-\infty}^{\infty}(T_L(E,\phi)f_o(E,\mu_L) - T_R(E,\phi)f_o(E,\mu_R))\,E\,\mathrm{d}E. \tag{57}$$

According to its symmetry properties, the transmission coefficients for both fluxes are identical, and thus we obtain

$$j_x = -\frac{4e}{h^2v_F}\int_{-\frac{\pi}{2}}^{\frac{\pi}{2}}\cos\phi\,\mathrm{d}\phi\int_{-\infty}^{\infty}T(E,\phi)\,(f_o(E,\mu_L) - f_o(E,\mu_R))\,E\,\mathrm{d}E. \tag{58}$$

In some cases, this general expression can be reduced, which could be useful in later work.

- If the existing bias is very large at low temperature, then the contribution due to the right reservoir, with a lower chemical potential, is negligible. It is possible to obtain the total density of current if we consider only the current provided by the reservoir on the left:

$$j_x = -\frac{4e}{h^2v_F}\int_{-\frac{\pi}{2}}^{\frac{\pi}{2}}\cos\phi\,\mathrm{d}\phi\int_{-\infty}^{\infty}T(E,\phi)f_o(E,\mu_L)E\,\mathrm{d}E. \tag{59}$$

- At low temperature ($k_BT < E_F - \mu$), when the electrons are highly degenerate, the Fermi function can be approximated by the step function, and therefore

$$j_x = -\frac{4e}{h^2v_F}\int_{-\frac{\pi}{2}}^{\frac{\pi}{2}}\cos\phi\,\mathrm{d}\phi\int_{\mu_R}^{\mu_L}T(E,\phi)E\,\mathrm{d}E. \tag{60}$$

- If the bias is very small, we can approximate the Fermi distribution by its Taylor approximation around the mean value of the chemical potentials $\mu = \frac{\mu_L+\mu_R}{2}$, and, considering that the difference between the chemical potentials is established in fact by means of the bias $\mu_L - \mu_R = e\,(V_R - V_L)$, we have

$$f_o(E,\mu_L) - f_o(E,\mu_R) \approx \frac{\partial f_o}{\partial\mu}(\mu_L-\mu_R) = e\frac{\partial f_o}{\partial\mu}(V_R-V_L) = -e\frac{\partial f_o}{\partial E}V_{DS} \tag{61}$$

and therefore

$$j_x = -\frac{4\mathrm{e}^2}{h^2v_F}V_{DS}\int_{-\frac{\pi}{2}}^{\frac{\pi}{2}}\cos\phi\,\mathrm{d}\phi\int_{-\infty}^{\infty}T(E,\phi)\left(-\frac{\partial f_o(E,\mu)}{\partial E}\right)E\,\mathrm{d}E. \tag{62}$$

- At ultra-low temperatures (at zero temperature $\mu = E_F$), we can approximate

$$-\frac{\partial f_o(E,\mu)}{\partial E} \approx \delta(E-\mu) = \delta(E-E_F) \tag{63}$$

such that in this approximation, we obtain

$$j_x = -\frac{4e^2}{h^2 v_F} V_{DS} E_F \int_{-\frac{\pi}{2}}^{\frac{\pi}{2}} T(E_F,\phi)\cos\phi \, d\phi. \tag{64}$$

In all the previous formulas, the minus sign describes the correct direction of the electrical current carried by both electrons and holes. In certain experimental measurements, the interest lies sometimes not so much in the current density, j_x, as in the conductance of the sample G. Since Ohm's law and the current intensity are

$$V_{DS} G = I = \int_0^W j_x \mathrm{d}y = j_x W \tag{65}$$

$$G_{\mathrm{eff}} = \frac{G}{W} = \frac{j_x}{V_{DS}}, \tag{66}$$

we may explicitly establish the *conductance per unit length* or *effective conductance* of the sample as

$$G_{\mathrm{eff}} = \left| \frac{4e}{h^2 v_F V_{DS}} \int_{-\frac{\pi}{2}}^{\frac{\pi}{2}} \cos\phi \, d\phi \int_{-\infty}^{\infty} T(E,\phi)\,(f_o(E,\mu_L) - f_o(E,\mu_R))\,E\,\mathrm{d}E \right|. \tag{67}$$

In particular, for the experimental conditions referred to above,

$$G_{\mathrm{eff}} \approx \frac{4e^2}{h^2 v_F} |E_F| \int_{-\frac{\pi}{2}}^{\frac{\pi}{2}} T(E_F,\phi)\cos\phi \, d\phi. \tag{68}$$

The sample conductance will depend on the potential applied to the top gate (through the transmission coefficient) and the potential applied to the back gate (through E_F). Different devices with different potential profiles will give rise to different transmission coefficients that must be determined in each case, but formula (68) will always be valid if the experimental conditions with which it was derived are maintained. In the near future, we intend to consider the application of the model proposed in this paper to study some of these possible devices.

6. Conclusions

In order to obtain an analytical description of the performance of some electronic devices with conduction channels in graphene by means of a formula that would enable the conductance of these devices and the variables that determine it, we have built a theoretical model that required an analysis of the Dirac model and the transport phenomena accompanying the electric conduction.

We have reviewed the characteristics of graphene that are necessary for a quantitative building of the model, and have posed and solved the Dirac ultrarelativistic equation for a two-dimensional electron in the presence of an external potential, which seems to characterize the conduction electrons in the graphene channel.

Modeling the external potential by a simple potential barrier, we have constructed the wavefunctions for this system and, from them, the reflection and transmission coefficients. We have built an *analytic closed expression* for them, whose dependence on the physical variables that govern the process is revealed in an express manner. These coefficients are determined by potential parameters, the height and width of the barrier, and electronic variables, the Fermi

energy and the angle of incidence. This magnitude is essential for the behavior of the system. Indeed, the transmission coefficient has a critical dependence on this variable: there is a limit angle, which depends on the energy and the potential, such that for higher incidence angles, the transmission coefficient falls to practically zero. For these values in the angle of incidence, the potential is almost opaque.

We thus considered another potential profile: two consecutive potential barriers, in general different. In this case, we also obtained the reflection and transmission coefficients *exactly* as functions of the parameters described. Also, in this case there may be a limit angle. The two barriers are independent and the phenomenon may occur in none, one or both barriers that conform the potential.

These results basically describe the behavior of an electron with specified characteristics in the system. However, the phenomenon of electrical conduction is due to a heterogeneous group of electrons whose statistical properties are known and are determined physically through gate potentials. The Landauer formalism, widely used to analyze these problems, directly relates the current density and the conductance of a sample to its transmission coefficient. However, the standard formulas are referred to systems in which the transmission coefficient is a constant, or independent of the direction. The fact that this coefficient is strongly anisotropic in our problem has made it necessary to review these formulas in this case.

We have also been able to build a rather general *closed expression* to describe the current density and conductance of these devices. This expression relates, through the transmission coefficient, the current density and the conductance of the sample to the physical parameters governing the problem and has already been mentioned. Finally, we have considered several simplifications that reproduce certain experimental conditions in order to find the ways taken by these magnitudes when an FET transistor under low polarization and at low temperature is considered. The experimental variables controlling the various magnitudes that determine the transmission coefficient, the current and the conductance of these devices are gate potentials. These determine the potential profile and Fermi energy of the carriers. This connection is a matter of great importance, hence our current interest. Its clarification would facilitate the control and design of new devices. Katsnelson and co-workers [11] stress that the fundamental problem in a standard single-layer graphene FET is that the conducting channel cannot be pinched off due to the Klein paradox. A single-layer graphene FET has been used experimentally as a test of the occurrence of Klein tunneling in graphene [13, 14]. Our results could help to design monolayer graphene transistors that could avoid this problem by using the angle dependence of the transmission coefficient. Our proposal has been to prepare a graphene FET with the top-gate at 22° with respect to the source and drain contacts. We have fabricated such a device and have obtained very promising results.

Acknowledgments

The authors acknowledge the support of this research by the DGICYT under project FIS2009-07880 and Fundación Samuel Solorzano under project FS/18-2012.

References

[1] Novoselov K S, Geim A K, Morozov S V, Jiang D, Zhang Y, Dubonos S V, Grigorieva I V and Firsov A A 2004 *Science* **306** 666
[2] Geim A K and Novoselov K S 2007 *Nature Mater.* **6** 183
[3] Wallace P R 1947 *Phys. Rev.* **71** 622
[4] Castro Neto A H, Guinea F, Peres N M R, Novoselov K S and Geim A K 2009 *Rev. Mod. Phys.* **81** 109

[5] Cerveró J M and Diez E 2011 *Int. J. Theor. Phys.* **50** 2134
[6] Dragoman D and Dragoman M 2007 *Appl. Phys. Lett.* **90** 143111
[7] Katsnelson M I, Novoselov K S and Geim A K 2006 *Nature Phys.* **2** 620
[8] Nguyen H C and Nguyen V L 2009 *J. Phys.: Condens. Matter.* **21** 045305
[9] Peres N M R 2009 *J. Phys.: Condens. Matter.* **21** 323201
[10] Calogeracos A 2006 *Nature Phys.* **2** 579
[11] Katsnelson M I and Novoselov K S 2007 *Solid State Commun.* **143** 3
[12] Beenakker C W J 2008 *Rev. Mod. Phys.* **80** 1337
[13] Stander N, Huard B and Goldhaber-Gordon D 2009 *Phys. Rev. Lett.* **102** 026807
[14] Young A F and Kim P 2009 *Nature Phys.* **5** 222
[15] Dragoman D 2009 *Phys. Scr.* **79** 015003
[16] Adam S, Hwang E H, Galitski V M and Das Sarma S 2007 *Proc. Natl Acad. Sci. USA* **104** 18392
[17] Milton Pereira J Jr, Vasilopoulos P and Peeters F M 2007 *Appl. Phys. Lett.* **90** 132122
[18] Biswas R, Mukhopadhyay S and Sinha C 2010 *Physica* E **42** 1781
[19] Bai C, Yang Y and Zhang X 2010 *Physica* E **42** 1431
[20] Milton Pereira J Jr, Vasilopoulos P and Peeters F M 2008 *Microelectron. J.* **39** 534
[21] Park C-H, Yang L, Son Y-W, Cohen M L and Louie S G 2008 *Nature Phys.* **4** 213
[22] Bliokh Y P, Freilikher V, Savelév S and Nori F 2009 *Phys. Rev.* B **79** 075123
[23] Novoselov K S, Geim A K, Morozov S V, Jiang D, Katsnelson M I, Grigorieva I V, Dubonos S V and Firsov A A 2005 *Nature* **438** 197
[24] Semenoff G W 1984 *Phys. Rev. Lett.* **53** 2449
[25] Landauer R 1988 *IBM J. Res. Dev.* **32** 306
[26] Landauer R 1992 *Phys. Scr.* **T42** 110
[27] Milton Pereira J Jr, Mlinar V, Peeters F M and Vasilopoulos P 2006 *Phys. Rev.* B **74** 045424
[28] Datta S 1995 *Electronic Transport in Mesoscopic Systems* (Cambridge: Cambridge University Press)
[29] Chuang S L 1995 *Physics of Optoelectronic Devices* (New York: Wiley)